



OPEN Preparation of ultramarine green pigments by recycling of the discarded molecular sieves for green vegetation spectral simulation

Haoyan Zhou^{1,2}, Mei Zu¹✉, Xinxuan Tang¹, Yuanxi Chang¹, Shiquan Li¹, Hongrui Yang¹, Chenglong Lv²✉ & Haifeng Cheng¹

Molecular sieves were widely used in the chemical industry, which caused a large number of inactivated molecular sieves to be discarded, resulting in a serious waste of resources and environmental pollution. Recently, recycling of discarded molecular sieves (DMS) has become a research hotspot. This study proposes an economical method using DMS to prepare green pigments mimicking foliage spectrum. The synthesized products were subjected to characterization using X-ray diffraction (XRD), Fourier-transform infrared spectroscopy (FTIR), Ultraviolet-visible-diffuse reflectance spectroscopy (UV-Vis-DRS), and scanning electron microscopy (SEM). The analysis revealed that sulfur radicals can be effectively incorporated as chromophores within the β -cages that are formed during the recrystallization process of sodalite, these cages are highly conducive to accommodating the radicals, thereby providing a protective environment that shields them from external influences. By adjusting the mass ratio of $\text{Na}_2\text{CO}_3/\text{S}$, the visible reflectance spectrum of ultramarine pigments can be easily modified. In addition, camouflage coating based on ultramarine green can be used to simulate the spectral reflectance characteristics of green vegetation. The Spectral Angle Mapping (SAM) system was used to evaluate the simulation effect of the camouflage coating. At a threshold below 98.5%, the camouflage coating still be misidentified as leaves, this method can recycle massive solid waste resources and significantly reduce the preparation cost of imitation green vegetation camouflage pigments.

Keywords Discarded molecular sieves, Spectral simulation, Ultramarine green pigments

With the rapid development of the global economy and society, industrial solid wastes from metal smelting¹, mineral extraction², power generation^{3,4} and other industrial wastes have proliferated and difficult to store and degrade, which will cause significant damage to the environment. Molecular sieves are crystalline aluminosilicates composed of oxygen-sharing SiO_4 and AlO_4 tetrahedra forming molecular sized channels and cavity systems, which provide zeolites a rich variety of properties and industrial potential applications related to adsorption⁵, separation and catalysis, etc. However, with the repeated application, a large number of inactive molecular sieves are produced⁶. It has been proven that the annual global output of discarded molecular sieves is as high as 0.5 to 0.7 million tons, making it one of the largest sources of industrial solid waste^{7,8}. Therefore, there is an urgent need for an effective method to utilize bulk DMS. The production of pigments from solid waste is an economical, safe, and environmentally friendly strategy that might be useful for this purpose^{9–11}. Generally, the chemical composition and microstructure of molecular sieves do not change during the participation in the catalytic reaction. Therefore, discarded molecular sieves retain a large number of silica-aluminum skeletons, which can be used as raw materials for the synthesis of ultramarine pigments. Ultramarine pigments have been used since as valuable pigments as early as the Middle Ages for its stable chemical properties, non-toxicity, excellent heat and light resistance. However, further development is limited due to the expensive price and the complicated

¹Science and Technology on Advanced Ceramic Fibers and Composites Laboratory, National University of Defense Technology, Changsha 410073, China. ²School of Physics and Optoelectronics Engineering, Xiangtan University, Xiangtan 411105, China. ✉email: zumei2003@163.com; lvchenglong@xtu.edu.cn

extraction process. The industrial manufacture of ultramarine pigments is currently quite common and cheap using kaolin, sulfur and soda as raw materials, and involves a simple thermal synthesis procedure. Meanwhile, some studies have shown that the substitution of zeolite for kaolin in the synthesis of ultramarine not only has the advantage of reducing the emission of SO_2 into the atmosphere, but also significantly broadens the range of product colors¹².

Green pigments are widely used in a variety of environmentally friendly products and in jungle camouflage because it is a common color in nature, where they are often used to cover objects to simulate the color of the background, helping to make objects visually invisible, thus counteracting the detection of optical instruments^{13,14}. Chlorophyll-like pigments are widely used to simulate spectral features of foliage, but they are unstable and prone to decomposition. Cr_2O_3 and CoCr_2O_4 , two common commercial inorganic green pigments, are widely used in camouflage applications as a replacement for chlorophyll due to their high coloring power and thermal stability^{15,16}. However, chrome pigments are toxic and add weight to the material. Gao et al. developed a bionic leaf with hygroscopic material and chrome oxide green as additives. Inspired by the structural features of leaves¹⁷, the spectral correlation coefficients between the bionic leaf and two kinds of leaves are over than 0.95. Xie et al. prepared a composite pigment for modelling green vegetation spectra by microencapsulation using encapsulated zinc phthalocyanine, but the environmental durability of the pigments is not explored in the article¹⁸. Although these camouflage materials achieve effective deception of detection equipment, application in real environments may be limited by complex preparation conditions and high costs.

In this work, we investigated the influence of the synthesis variables on the structure and color of the ultramarine products and explored the environmental stability and camouflage properties of the camouflage coatings. Preparation of ultramarine green pigments from DMS which can not only expands the range of colors available in ultramarine pigments, but also further reduce costs and environmental pollution. Moreover, these inorganic non-metallic pigments are expected to replace cobalt green, chrome green and other metallic colors in the camouflage pigments from the perspective of the economy and environmental protection.

Materials and methods

Materials

The DMS sample used in this study was obtained from Inner Mongolia Xitai regeneration resource treating Co. Ltd (Inner Mongolia, China), which is a company that comprehensively utilizes the waste resources of industrial waste catalysts and metal-containing wastes. Anhydrous sodium carbonate (Na_2CO_3 , $\geq 99\%$) was purchased from Shanghai Meryer Chemical Technology Co. Ltd (Shanghai, China). Polyvinyl alcohol 124 ($[\text{C}_2\text{H}_4\text{O}]_n$, GR grade) was purchased from Beijing Wokai Biotechnology Co. Ltd (Beijing, China). Anhydrous lithium chloride (LiCl , $\geq 99\%$), sulfur (S , $\geq 99.5\%$) was purchased from Shanghai Aladdin Biochemical Technology Co. Ltd (Shanghai, China). Rosin ($\geq 90\%$) was purchased from Cangzhou Lite Equipment Co. Ltd (Cangzhou, China). All chemical reagents were analytical reagent and used without any further purified, the experiments were performed with homemade deionized water from the laboratory.

Experimental methods

Pretreatment of discarded molecular sieves

As starting materials, the DMS were dispersed in an ultrasonic water bath and then calcined in a muffle furnace at 300 °C for 2 h to remove the water-soluble impurities and organic additives from them, to obtain purified DMS and sieved (300 mesh). Then, they were cooled at room temperature and kept in a desiccator before use for pigment synthesis.

Preparation of the ultramarine green

After pretreatment, 2.5 g DMS, 0.5 g rosin, 1 g sulfur and 0.25 g, 0.5 g, 1 g, 1.5 g, 2 g, 2.5 g Na_2CO_3 were mixed in an agate mortar (The elemental sulfur was employed as radical precursor in all experiments and its content in the initial mixture always made 40 wt% of zeolite), then the ground powder was transferred into a covered ceramic crucible. The mixture was heated to 400 °C at a heating rate of 5 °C/min and held for 1 h, in order to facilitate the reaction of melt sulfur with sodium carbonate to form the sodium polysulfide. And then the mixture was continuously heated at temperature of 600–800 °C for 1–2 h. The growing alkalinity in the series was attained by adding an increasing amount of Na_2CO_3 , by controlling the mass ratio of $\text{Na}_2\text{CO}_3/\text{S}$ in the feedstock to generate different concentrations of radicals. The crude product of ultramarine product obtained from the reaction was ground to obtain a powder sample when the samples were cooled to room temperature, then washed and filtered with a concentration of 2% chloroform solution at 80 °C, next washed several times with deionized water at 60 °C to obtain purified ultramarine green.

Preparation of camouflage coating

The camouflage coating was prepared by solution casting method, polyvinyl alcohol (PVA) powder was dissolved in 90 °C water with stirring in the ratio of 1:9, and then ultramarine pigment and lithium chloride (LiCl) particles were added sequentially, finally the configured solution was poured on the polished aluminum plate, and solidified at 60 °C in the drying oven for 10 h.

Characterization techniques

The following methods were used to characterize the sample that was obtained throughout our experiments. X-ray Diffraction (XRD) and Fourier Transform infrared (FTIR) spectroscopy were used to observe the modifications of the sample structure upon calcination. The XRD analysis of the sample was recorded using the Bruker D8 Advance X-ray diffractometer, using $\text{Cu-K}\alpha$ ($\lambda = 1.5418 \text{ \AA}$, 40 kV, 40 mA) radiation, scanning range

of 5°–80° and scanning rate of 5°/min. The FTIR was recorded on Bruker Vertex 70 produced by transform infrared spectrophotometer in the 4000–400 cm^{−1} wavenumber range on instrument spectrophotometer in KBr discs. The X-ray Fluorescence (XRF, Rigaku ZSX primus, Japan) analyzer was used to analyze the chemical compositions of DMS tested. The surface morphology and microstructure of the samples were observed by Hitachi SU8100 scanning electron microscope (SEM, Japan) equipped with an energy dispersion spectrometer (EDS), and the samples were prepared by attaching powder to standard aluminum SEM stubs using carbon tape in order to improve the electrical conductivity. Images were collected at a voltage of 3 and 5 kV. The thermogravimetric analysis (TGA, NETZSCH, Germany) was used for the analysis of the thermal property of samples. The experiment was collected by NETZSCH TGA209F1 in the temperature range of 30–1000 °C at a heating rate of 10 °C/min in the ambient atmosphere. The Raman spectrum of the samples was recorded using Renishaw inVia Raman microscope (UK), with a Raman shift of 1800 to 400 cm^{−1}. The particle size distribution was obtained by LS-909 OMEC laser particle size analyzer (China), the pigments were immersed in anhydrous ethanol and ultrasonically dispersed for 10 min before the particle size distribution of the powder was tested using a particle size analyzer. UV–VIS absorption-reflectance spectroscopy is the predominant tool used to distinguish the light reflection characteristics of pigments. The color of pigments is caused by the selective absorption and reflection of some wavelengths of visible light. Namely, the higher the reflectivity at a certain wavelength, the color in this wavelength range will appear. Reflectance spectra and ultraviolet-visible diffuse reflectance spectra of the samples were measured by PerkinElmer Lambda 1050 + UV-Vis-NIR spectrophotometer (America) combined with a 150 mm diameter integrating sphere detector in the wavelength range of 250–2500 nm, using a polytetrafluoroethylene white plate as the standard sample. The colorimetric method CIE 1931 LAB was utilized to characterize the color of pigments. L* is the brightness of the pigment, b* represents the blue color, with a high negative value representing a strong blue intensity, and a* represents the green color, with a positive value representing red and a negative value representing green, and the color coordinates were obtained based on reflectance spectral data by conversion of the Color Tell tool (calculated spectral range was 380–760 nm).

The similarity between the reflectance spectral profiles of the camouflage coating and the green vegetation can be characterized by the spectral similarity equation:

$$\gamma_{xy} = \frac{\sum_{i=1}^m (x_i - \bar{x}_I)(y_i - \bar{y}_I)}{\sqrt{\sum_{i=1}^m (x_i - \bar{x}_I)^2} \sqrt{\sum_{i=1}^m (y_i - \bar{y}_I)^2}} \quad (1)$$

Where x_i and y_i represent the spectral value of measured sample and reference sample at a wavelength of i .

$\bar{x}_i = \sum_{i=1}^m x_i$ and $\bar{y}_i = \sum_{i=1}^m y_i$ are the respective average value of reflectivity spectrum in the tested wavelength range, respectively. The samples were tested in the range of 400–2500 nm, test band width is 5 nm. γ_{xy} expresses the similarity between the two spectra, the range of γ_{xy} is [−1, 1], and the larger the absolute value of γ_{xy} presents the more spectral similarity between the reference and the test sample.

Absorption limits are defined by the Kubelka–Munk formula:

$$F(R) = \frac{(1 - R)^2}{2R} \quad (2)$$

where R is the absolute reflectance at each wavelength.

Results and discussion

The chemical analyses and XRD patterns of the DMS are given in Table 1 and Fig. 1a, respectively. The principal phase in the DMS product was FAU topology. It is a hydrated aluminum silicate composed of alkali metals and alkaline earths, with porous characteristics favorable to the production of ultramarine pigments. Chemical composition analysis showed that DMS had a considerable amount of SiO₂ (47.1 wt%) and Al₂O₃ (30.7 wt%) and the total concentration of Fe₂O₃ and K₂O was less than 1%, indicating a suitable raw material for the synthesis of ultramarine green (Na₈[AlSiO₄]₆(S₂S₃)₂).

Effects of synthetic conditions on ultramarine

calcination conditions. The documentation of zeolite structural transformations during thermal treatment of polysulfides is an important part of product characterization. As shown in Fig. 1a, increasing the calcination temperature can lead to the transformation of structure. When the calcination temperature was lower than 700 °C, the samples retained the characteristic diffraction peaks of the DMS structure, with increasing calcination temperature and time, the characteristic diffraction peaks belonging to the zeolite faujasite (FAU) framework disappeared and new peaks of the sodalite (SOD) structure appeared at 13.88, 24.19 and 34.47 as the

Component	SiO ₂	Al ₂ O ₃	Na ₂ O	CaO	K ₂ O	Fe ₂ O ₃
Content (wt%)	47.1%	30.7%	15.7%	2.7%	0.7%	0.2%

Table 1. Chemical compositions of the DMS in this study (wt%).

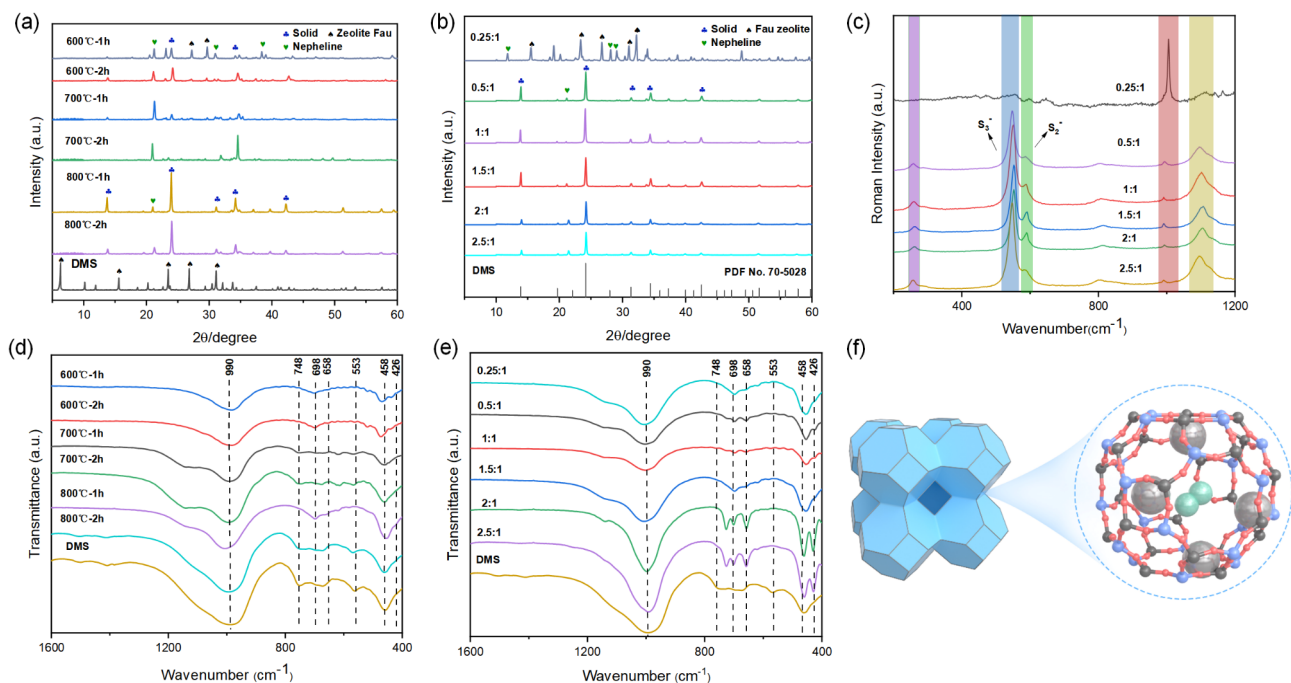


Fig. 1. The XRD pattern corresponding to (a) different heat-treatments condition and (b) different mass ratio of $\text{Na}_2\text{CO}_3/\text{S}$; (c) Raman spectra of the synthesized sample; FTIR spectrum of (d) different heat-treatments condition and (e) different mass ratio of $\text{Na}_2\text{CO}_3/\text{S}$; (f) Structural of ultramarine green pigments. The β -cage (right) is a unit cell of the framework and spheres represent Si (blue) Al (grey) and S_2^- (green).

temperature rising above 700°C ¹⁹. The peaks of the FAU structure completely disappeared in the sample calcined at 800°C for 1 h. All diffraction peaks of the obtained samples are in good corresponded with the standard card of ICCD PDF No. 70-5028 (corresponding to the ultramarine pigment). Notably, the SOD structure remains intact even at temperatures as high as 800°C , which is significantly higher than the decomposition temperature of bare zeolite²⁰. It is possible that the alkali source acts as a structural guide while protecting the cage from disintegration. Therefore, to maintain high crystallinity and purity without affecting the pigment performance, calcining conditions of 1 h at 800°C were selected. Fig. 1b illustrates the changes in the XRD pattern spectra of the samples prepared with varying concentrations of Na_2CO_3 . At low alkalinity levels, the discarded molecular sieves (DMS) retain their FAU structure and mix with a nepheline structure, resulting in a non-colored sample. The intensity of the diffraction peaks is observed to increase initially and then decrease with increasing alkalinity. Notably, no additional peaks are present that could be attributed to other phases^{12,21}.

Figure 1c presents Raman spectra of the synthesized sample. The band near 262 cm^{-1} is assigned to the bending mode of containing mainly 4-membered rings, and the band at $900\text{--}1100\text{ cm}^{-1}$ can be assigned to the asymmetric stretching modes of T-O for amorphous aluminosilicates²². The presence of trace elemental impurities in DMS will lead to an increase in the fluorescence background, resulting in a drift in the Raman signals. Color in ultramarines comes from the encapsulation of specific sulfur species. Specifically, both radical chromophores are Raman active and their vibrational bands have been assigned by Raman spectroscopy at 550 cm^{-1} and 590 cm^{-1} for blue and yellow, respectively. These peaks are considered to be the fingerprint peaks of ultramarine pigments.

Changes in functional groups ultramarine zeolite synthesis. Further evidence supporting the sodalite structure of the synthesized ultramarine pigment was obtained from the FT-IR spectra (Fig. 1d-e). The quintessential shoulder peaks at around 990 cm^{-1} are assignable to asymmetric stretching vibration peaks of TO_4 (T = Si, Al), 558 cm^{-1} is the characteristic peak of single four-ring (S4R) and one of the major (secondary structural units) SBU in the structure of sodalite²³, and the intensity of the absorption peaks can be used as an important symbol for judging the growth of sodalite. Additionally, when the content of $\text{Na}_2\text{CO}_3/\text{S}$ was 0.25, the sodium-aluminum silicate in the amorphous product at 698 cm^{-1} , 658 cm^{-1} split to produce weaker characteristic peaks. The intensity of the characteristic peaks decreased slightly with increasing alkalinity, indicating that the characteristic peaks of (double six-ring) D6R in disappeared, that the structure of the structure was disintegrated, and the characteristics of the peaks of the sodalite peaks complete stronger (553 , 458 and 426 cm^{-1}), indicating that in the process of sodalite formation alkalinity is an important factor in its structural transformation.

Analysis of the color mechanism of ultramarine pigments. Ultramarine is an aluminosilicate sodalite structures containing sulfur chromophores²⁴, the reaction between sulfur and alkali compounds produces chromophore groups that diffuse into the zeolite cages and become encapsulated in the zeolitic structure. Specifically, the formation of different color species is affected by the geometry and size of the zeolite cage as well as the preparation conditions. The sodalite units within the ultramarine structure are directly interconnected, with the colorless framework serving as a cage capable of encapsulating small ions and molecules^{22,25,26} (Fig. 1f).

The embedment of the sulfur radicals inside the sodalite units provides them very good protection, and results in very high stability of the ultramarine pigments. This bears some resemblance to the cellular structure of plants that provides a living environment for phytochromes.

Microstructure changes of synthesized ultramarine pigments. Figure 2 provides information about the morphology of calcined powder samples (U1-U6). It can be observed from the SEM images that all the samples exhibit a certain degree of agglomeration. The agglomerated particles are not uniform in size, ranging in size from 1 to 3 μm . Most of the crystals retain the cubic structure of DMS under low alkalinity. With the mass fraction of Na_2CO_3 increase, the morphology of the products became irregular and clustered, accompanied by an increase in size²³. Meanwhile, EDS analysis showed that the S chromophores were uniformly distributed in the ultramarine pigments.

After thermal treatment of the mixtures in the muffle furnace with a reducing atmosphere, pigments of different colors were obtained. To observe the chromaticity distribution of pigments more intuitively, the chromaticity coordinates of synthetic pigments are plotted on the CIE1931 chromaticity diagram. The changes in alkalinity affected not only the structure of the products, but also their color. The color of sample calcination in low alkalinity exhibits sepia or gray-black color (Fig. 3a-b). As the content of Na_2CO_3 increases, the L^* value shows a trend of increasing and then decreasing, and the overall trend of the a^* value is gradually decreasing, indicating that the green color content in the samples is gradually increases. The U4 exhibits a blue-green color when the $\text{Na}_2\text{CO}_3/\text{S}$ ratio is 1.5, and green specimen prepared at twice stoichiometric ratio of $\text{Na}_2\text{CO}_3/\text{S}$ exhibited the lowest a^* value (-17.5) value in the CIE LAB color space.

From Fig. 3c shows the diffuse reflectance spectra (DRS) obtained for thermally obtained ultramarine. The DRS spectra of the U1 do not show any absorption. With the transition to the ultramarine pigment structure, the sample begins to show absorption at 600 nm and 390 nm, which can be attributed to the S_3^- and S_2^- radicals, respectively. The chromophore species are sulfur anion radicals, which produce different colors in the final product. With the increase of Na_2CO_3 content, the intensity of the peaks at 380 nm indicates that more S_2^- radicals are formed, this is due to the fact that S reacts with Na_2CO_3 at high temperature in the molten state to form sodium polysulfide, and then through the continuous reaction of S-S bond dissociation of sodium polysulfide to

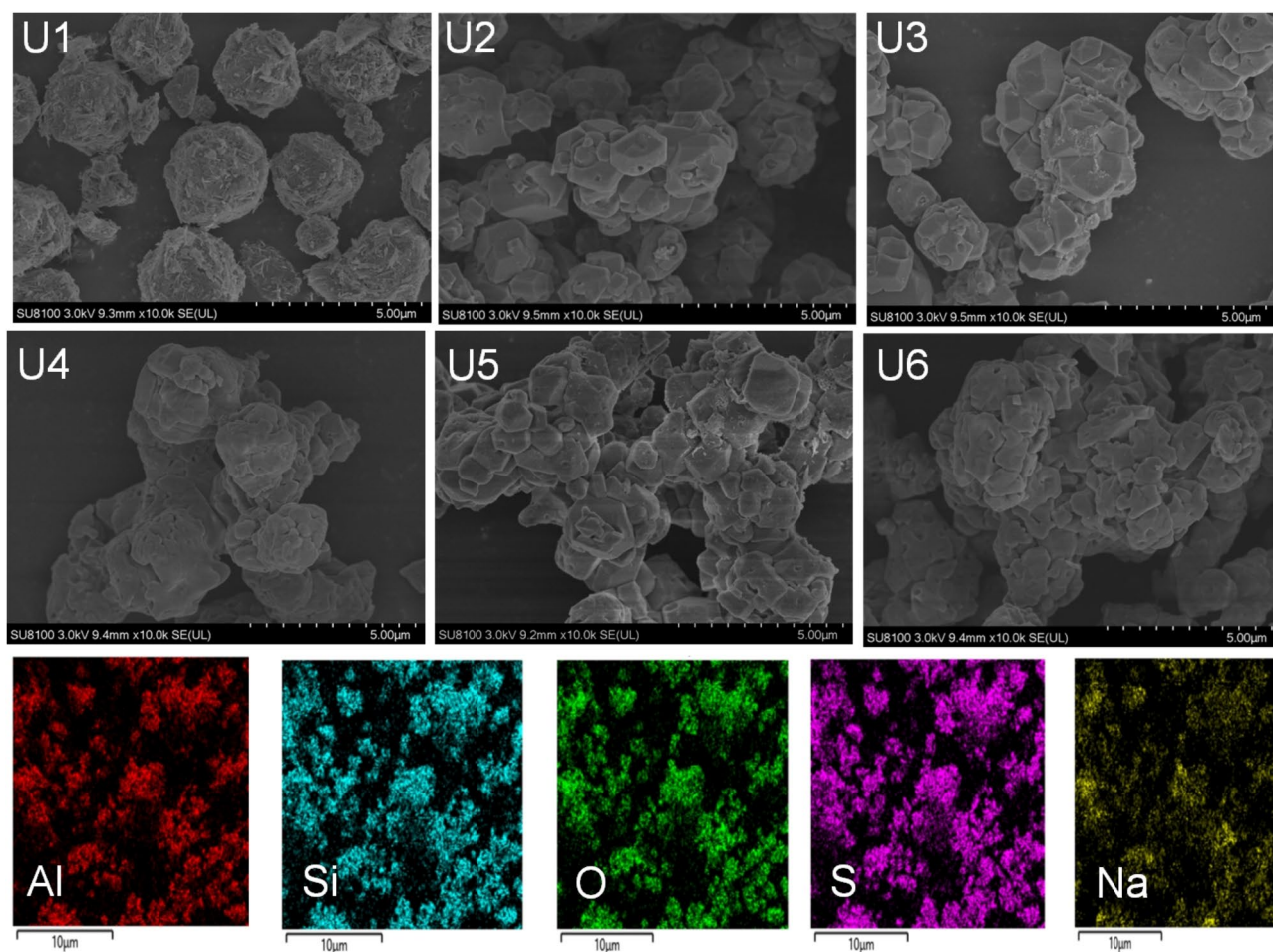


Fig. 2. SEM images of the synthesized ultramarine pigment and the corresponding elemental mapping of Al, Si, O, S, Na (The different $\text{Na}_2\text{CO}_3/\text{S}$ mass ratios of 0.25, 0.5, 1, 1.5, 2, 2.5 used for ultramarine pigments synthesis were denoted as U1-U6).

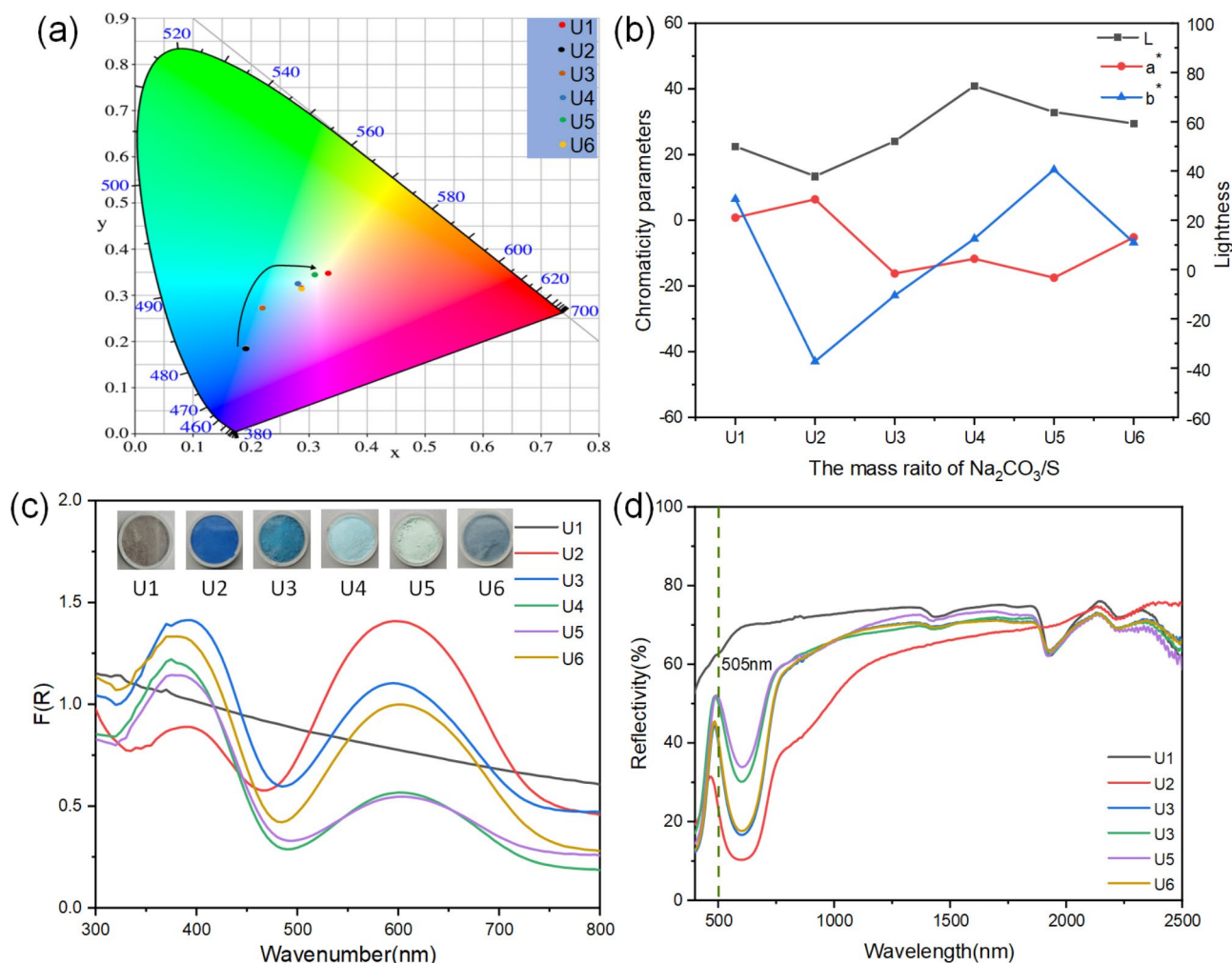


Fig. 3. (a) Chromatic CIE1931 coordinates in the standard color space of ultramarine pigment; (b) The diagram of CIE L*a*b* values of ultramarine pigment; (c) Diffuse reflectance spectra and (d) Vis-NIR reflectance spectrum of ultramarine pigment.

form chromophores, which finally migrate to the β -cage of the ultramarine skeleton, thus producing color in the pigment. Excessive Na_2CO_3 ensures sufficient sulfur reaction to produce substantial amounts of polysulfides. However, the S_2^{2-} produced by its cleavage cannot be fully oxidized to S_3^{2-} within a short period of time, resulting in a large number of residual yellow chromophores in the sample, leading to a lesser $\text{S}_3^{2-}/\text{S}_2^{2-}$ ratio. The lower the ratio, the pigment leans towards the green hue. On the other hand, the integrity of the ultramarine skeleton determines the amount of sulfur that can be incorporated inside the structure.

Figure 3d depicts the visible-near-infrared (Vis-NIR) spectra of the samples, it was found that the prepared ultramarine pigments have certain similarity to natural leaves with a high reflectance plateau at 780–1300 nm. However, at a low mass content of Na_2CO_3 , the visible light reflectance peak of ultramarine (U1–U3) is located in the blue region, with spectral characteristics that are greatly different from the green plants. When the relative ratio of $\text{Na}_2\text{CO}_3/\text{S}$ is increased from 0.5 (U2) to 2 (U5), the center position of the reflectance peak of ultramarine pigments shifts from 460 to 505 nm, and the intensity of the reflectance peak increases from 31.8 to 48.9%, which is close to the “green peak” of the green foliage. In addition, the decrease in reflectance in the near-infrared region can be attributed to the increase in alkalinity, which leads to the deterioration of crystallinity and an increase in particle size of ultramarine pigments.

Properties and applications of camouflage coatings

Spectral properties of camouflage coatings. Hyperspectral detection technology combines the advantages of spectral analysis and remote sensing imagery. By extracting sensitive scene spectral information and identifying the spectral differences between suspicious targets and background features, it can reveal different environmental targets and pose a significant threat to the survivability of camouflaged military targets. Green vegetation, as one of the most common backgrounds on the land, it has a unique spectral profile that traditional camouflage materials can only achieve visible spectral characteristics with the vegetation background^{18,27}. Therefore, the investigation of novel materials for simulating of green vegetation spectrum assumes considerable significance.

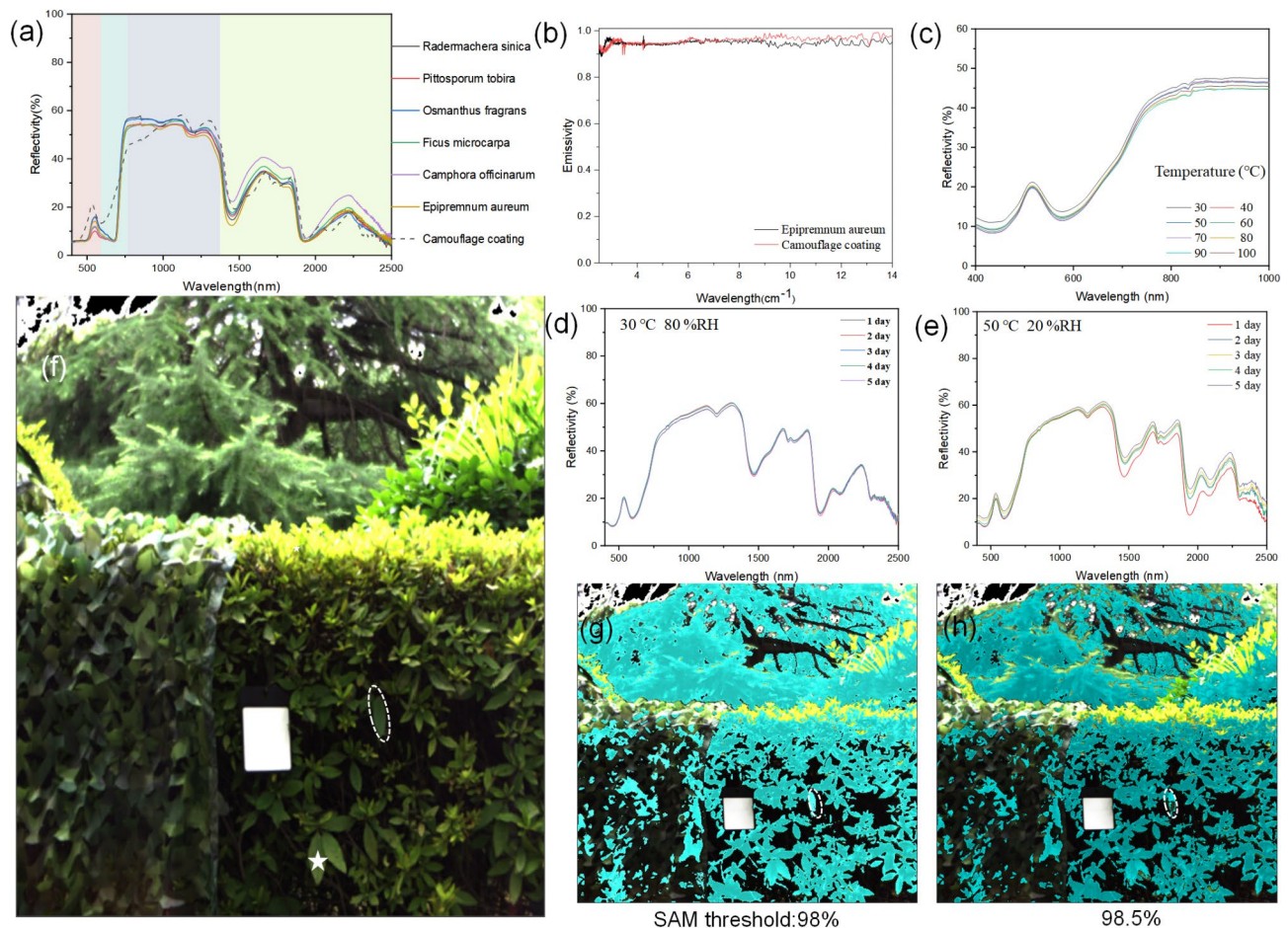


Fig. 4. (a) Vis-NIR reflectance spectrum of common plant leaves and camouflage coatings; (b) Infrared emissivity of camouflage coating and *Epipremnum* leaf; (c) The reflectance spectra of camouflage coatings in the 400–1000 nm band as temperature increases (measured by hyperspectral camera); (d) Humid (30 °C, 80%RH) and (e) dry (50 °C, 20%RH) environments for 5 days reflectance spectra of the coating; (f) Camouflage coating photographed under hyperspectral camera (Left is commercial camouflage netting, right is camouflage coating attached to a branch of bush); (g–h) Hyperspectral photographs at different SAM thresholds (Reference pixels are marked with an asterisk).

The reflectance areas in the Vis-NIR band (400–2500 nm) of various green vegetation species have similar characteristics, the typical reflectance spectral curves of several green vegetation species in southern China are shown in Fig. 4a. It can be seen that the Vis-NIR reflectance spectral curves of green vegetation leaves have four main features, the “green peak” refers to the weak reflectance peak at 550 nm, and the “red edge” in the interval of 680–750 nm, which the reflectance spectral curve increases rapidly forming a steeply sloping edge. In the near-infrared region of 780–1300 nm, the overall reflectance is high and tends to be level, so it was called the “near infrared plateau”. The two noticeable absorption peaks are located in 1460 nm and 1940 nm, which are associated with the large amount of water in plant leaves. Compared to natural plants, the spectral curves of ultramarine green in the visible band exhibit similar characteristics. In contrast, the spectral shapes in the near-infrared region show slight differences, primarily due to the absence of double frequency absorption in the 1400–2500 nm region.

Although the prepared ultramarine green pigments exhibited similar spectral characteristics to green leaves in the visible region, their overall spectral reflectance in the NIR was significantly higher than that of natural leaves. Following the above-reported results, coating samples were prepared using U5 samples and their reflectance spectra were evaluated. the camouflage coatings were prepared via a solution casting method with polyvinyl alcohol (PVA) and lithium chloride (LiCl) to imitate the Vis-NIR spectra and thermal infrared characteristics of green vegetation, PVA is a transparent polymer material with good membrane forming performance and mechanical properties. The prepared camouflage coatings showed similar characteristics to healthy green leaves, consisting of “green peak”, and “red edge” at 400–780 nm band, and reflectivity of 20.1% and 19.3% at water absorption peak, respectively. The results of the calculations show that the correlation coefficient of spectrum shape between the camouflage coatings and the green leaves of *Radermachera sinica*, *Pittosporum tobira*, *Osmanthus fragrans*, *Ficus microcarpa*, *Camphora officinarum*, and *Epipremnum aureum* are 0.95, 0.94, 0.94, 0.94, 0.95, and 0.95 in the 400–2500 nm band, respectively. Thermal infrared detectors are often used in

conjunction with hyperspectral detection on the modern battlefield, which makes multi-band camouflage of the solar and infrared spectra challenging, therefore the simulation of the thermal infrared characteristics of the blades is also necessary, it mainly depends on the infrared emissivity and temperature. As shown in Fig. 4b, the emissivity of the coating is 0.95, similar to that of plant leaves, and from the thermal infrared images it can be seen that the camouflage coatings have almost the same thermal infrared properties as the background, suggesting that the materials also have a certain camouflage potential when dealing with reconnaissance means at infrared wavelengths as well (Fig. S5).

At the same time, camouflage materials need to maintain their spectral properties in the application environment, based on which the stability of the camouflage coatings in a simulated jungle environment was tested. The thermogravimetric analysis of Fig. S4 previously showed that ultramarine pigments have good thermal stability, and this thermal stability was inherited to the camouflage coatings (Fig. 4c). The reflectance spectra of the coatings remained almost unchanged at temperatures up to 100 °C, and although a slight decrease in reflectance of the near-infrared plateau feature could be observed at higher temperatures, the overall reflectance of the coatings was still higher than 45%. In addition, in the simulated jungle environment with high humidity and different temperatures, the coating did not show significant spectral changes within 5 days, which suggests that the camouflage coating may have good stability and certain potential for application in real jungle environments (Fig. 4d–e).

Coating camouflage performance verification. Furthermore, to assess the camouflage performance of the coating, we conducted a comparison between our coating and commercially available camouflage textiles against a natural feature-rich backdrop. Visually, the coating exhibited a high degree of resemblance to plant foliage (Fig. 4f). The camouflage performance was quantitatively validated using a hyperspectral imaging camera in conjunction with Spectral Angle Mapping (SAM), a classification technique that determines spectral similarity by assessing the angular relationship between the spectrum of the test pixel and a reference spectrum. The results indicated that a substantial area of the camouflage netting was categorized as a non-leaf object, with a classification rate below the 98% threshold, indicative of a camouflage failure. In contrast, the coating maintained effective concealment within the forested setting. As the threshold is further increased to 98.5%, the mask becomes smaller and the specimens remain partially indistinguishable from the background (Fig. 4g–h). This further suggests that the camouflage coating prepared in presents work have highly similar spectral characteristics to the green vegetation.

Conclusions

In summary, the present work proposes a low-cost and sustainable method to prepare camouflage pigment derived from discarded molecular sieves. The effects of different $\text{Na}_2\text{CO}_3/\text{S}$ mass ratios and heat treatment conditions on the phase structure, morphology, color and optical properties of ultramarine pigments were systematically analyzed. The product that retains the parent structure will not be colored, and attain certain temperature and alkalinity conditions FAU recrystallizes to form the SOD structure, which is ideally containers suited to accommodate chromophores and protect them from environmental influences. Stable green pigments based on sulfur chromophores supported on DMS have been synthesized when the $\text{Na}_2\text{CO}_3/\text{S}$ mass ratio is equal to 1.5 or 2. The deep green color is presented when the $\text{Na}_2\text{CO}_3/\text{S}$ mass ratio is 2 times. Based on the results, ultramarine green with optimal spectral properties was prepared as a pigment, lithium chloride was used to modify the water absorption properties of the coating, and polyvinyl alcohol was used as a matrix to prepare a spectral coating mimicking green vegetation, the correlation coefficient of spectrum shape between the camouflage coating and green plant in the whole range of 400–2500 nm is as high as 0.95, demonstrated a strong spectral similarity. Moreover, the superior capabilities of hyperspectral camouflage are demonstrated by using spectral classification algorithms in practical forest scenarios. The conversion of industrial solid wastes into camouflage materials not only solves the environmental problems caused by the storage of industrial solid wastes, but also reduces the cost of producing camouflage pigments and generates certain economic benefits.

Data availability

The datasets generated during and/or analyzed during the current study are available on reasonable request, by contacting the corresponding author.

Received: 29 October 2024; Accepted: 18 February 2025

Published online: 12 March 2025

References

- Collins, F., Rozhkovskaya, A., Outram, J. G. & Millar, G. J. A critical review of waste resources, synthesis, and applications for zeolite LTA. *Microporous Mesoporous Mater.* **291** <https://doi.org/10.1016/j.micromeso.2019.109667> (2020).
- Hosseini Asl, S. M. et al. Porous adsorbents derived from coal fly Ash as cost-effective and environmentally-friendly sources of aluminosilicate for sequestration of aqueous and gaseous pollutants: A review. *J. Clean. Prod.* **208**, 1131–1147. <https://doi.org/10.1016/j.jclepro.2018.10.186> (2019).
- Ujaczki, E. et al. Re-using bauxite residues: benefits beyond (critical raw) material recovery. *J. Chem. Technol. Biotechnol.* **93**, 2498–2510. <https://doi.org/10.1002/jctb.5687> (2018).
- Qiu, Y., Wu, D., Yan, L. & Zhou, Y. Recycling of spodumene slag: Preparation of green polymer composites. *RSC Adv.* **6**, 36942–36953. <https://doi.org/10.1039/c6ra03119f> (2016).
- Wang, Y., Du, T., Jia, H., Qiu, Z. & Song, Y. Synthesis, characterization and CO₂ adsorption of NaA, NaX and NaZSM-5 from rice husk Ash. *Solid State Sci.* **86**, 24–33. <https://doi.org/10.1016/j.solidstatesciences.2018.10.003> (2018).
- Abdelrahman, E. A. Synthesis of zeolite nanostructures from waste aluminum cans for efficient removal of malachite green dye from aqueous media. *J. Mol. Liq.* **253**, 72–82. <https://doi.org/10.1016/j.molliq.2018.01.038> (2018).

7. Shi, P., Li, Z., Chen, X., Zeng, L. & Hu, R. Effect of industrial waste molecular sieves on internally cured cement-based materials. *Front. Mater.* **9** <https://doi.org/10.3389/fmats.2022.1003556> (2022).
8. Teng, L. et al. Facile and fast synthesis of cancrinite-type zeolite from coal fly Ash by a novel hot stuffy route. *J. Environ. Chem. Eng.* **10** <https://doi.org/10.1016/j.jece.2022.108369> (2022).
9. Menezes, R. A. et al. Synthesis of ultramarine pigments from Na-A zeolite derived from Kaolin waste from the Amazon. *Clay Miner.* **52**, 83–95. <https://doi.org/10.1180/claymin.2017.052.1.06> (2018).
10. Menezes, R. A., d., Paz, S. P. A., d., Angélica, R. S., Neves, R. & Pergher, S. B. C. Color and shade parameters of ultramarine zeolitic pigments synthesized from Kaolin waste. *Mater. Res.* **17**, 23–27. <https://doi.org/10.1590/s1516-14392014005000078> (2014).
11. Tajer Kajinebaf, V., Rezaeian, F., Rajabi, M. & Baghshahi, S. Replacing nano-clay for Kaolin in ultramarine pigments. *Pigm. Resin Technol.* **43**, 1–7. <https://doi.org/10.1108/prt-03-2013-0020> (2013).
12. Wang, H. et al. A systematic study of the synthesis conditions of blue and green ultramarine pigments via the reclamation of the industrial zeolite wastes and agricultural rice husks. *Environ. Sci. Pollut. Res. Int.* **27**, 10910–10924. <https://doi.org/10.1007/s11356-020-07624-8> (2020).
13. Basnayake, S. A., Tan, K., Leonard, M., Chabal, Y. & Balkus, K. J. Encapsulation of red sulfur chromophores in a zeolitic imidazolate framework (ZIF-8) via solvent assisted linker exchange. *Microporous Mesoporous Mater.* **219**, 172–177. <https://doi.org/10.1016/j.micromeso.2015.08.010> (2016).
14. Xu, C. et al. Design, Preparation and performance evaluation of core unit in multispectral camouflage coating. *Infrared Phys. Technol.* **121** <https://doi.org/10.1016/j.infrared.2021.104013> (2022).
15. Ai, S., Zheng, H. & Yu, J. Preparation and reflectance spectrum modulation of Cr₂O₃ green pigment by solution combustion synthesis. *Materials* **13** <https://doi.org/10.3390/ma13071540> (2020).
16. Xie, D., Luo, Q., Zhou, S., Zu, M. & Cheng, H. One-step Preparation of Cr₂O₃-based inks with long-term dispersion stability for inkjet applications. *Nanoscale Adv.* **3**, 6048–6055. <https://doi.org/10.1039/d1na00244a> (2021).
17. Gao, Y. & Ye, H. Bionic membrane simulating solar spectrum reflection characteristics of natural leaf. *Int. J. Heat Mass Transf.* **114**, 115–124. <https://doi.org/10.1016/j.ijheatmasstransfer.2017.06.051> (2017).
18. Xie, D. et al. A hyperspectral camouflage colorant inspired by natural leaves. *Adv. Mater.* **35**, e2302973. <https://doi.org/10.1002/adma.202302973> (2023).
19. Škvarlová, A. et al. Preparation and characterization of ultramarine blue pigments from fly Ash by using the X-ray photoelectron spectroscopy (XPS) for the determination of chemical States of sulphur in chromophores. *Microporous Mesoporous Mater.* **284**, 283–288. <https://doi.org/10.1016/j.micromeso.2019.04.039> (2019).
20. Raulin, K. et al. Identification of the EPR signal of S(2)(-) in green ultramarine pigments. *Phys. Chem. Chem. Phys.* **13**, 9253–9259. <https://doi.org/10.1039/c0cp02970j> (2011).
21. Wang, H., Zhen, Z., Yao, S. & Li, S. Synthesis of high acid-resistant ultramarine blue pigment through coal Gangue, industrial zeolite waste and corn straw waste recycling. *Resour. Chemicals Mater.* **1**, 137–145. <https://doi.org/10.1016/j.recm.2022.03.003> (2022).
22. Cato, E., Rossi, A., Scherrer, N. C. & Ferreira, E. S. B. An XPS study into sulphur speciation in blue and green ultramarine. *J. Cult. Herit.* **29**, 30–35. <https://doi.org/10.1016/j.culher.2017.09.005> (2018).
23. Shen, F. & Chen, H. The Preparation and characteristics of a blue pearlescent pigment with LTA-Type ultramarine coated on the Mica substrate. *Nano* **16** <https://doi.org/10.1142/s179329202150065x> (2021).
24. Borhade, A. V., Kshirsagar, T. A. & Dholi, A. G. Novel synthesis of ultramarine blue from waste coal fly Ash via thiocyanate aluminosilicate sodalite. *J. Sulfur Chem.* **37**, 632–645. <https://doi.org/10.1080/17415993.2016.1173215> (2016).
25. Chivers, T. Ubiquitous trisulphur radical ion S₃[−]. *Nature* **252**, 32–33. <https://doi.org/10.1038/252032a0> (1974).
26. Kowalak, S. & Jankowska, A. Transformation of zeolite structures during synthesis of ultramarine analogues. *Eur. J. Mineral.* **17**, 861–867. <https://doi.org/10.1127/0935-1221/2005/0017-0861> (2006).
27. Lv, C., Zu, M., Xie, D. & Cheng, H. Emulating solar spectral reflectance of natural leaf with bionic leaf prepared from 4A Zeolite-Derived ultramarine green pigment. *Mater. (Basel)*. **14**. <https://doi.org/10.3390/ma14061406> (2021).

Author contributions

Conceptualization – Mei Zu(lead), Haoyan Zhou (equal). Methodology – Haoyan Zhou(lead), Hongrui Yang (supporting), Shiquan Li(supporting). Writing – original draft – Haoyan Zhou (lead), Xinxuan Tang (supporting), Hongrui Yang(supporting). Writing – review & editing – Haoyan Zhou (lead), Mei Zu (supporting), Yuanxi Chang(supporting), Chenglong Lv(supporting), Haifeng Cheng (supporting).

Declarations

Competing interests

The authors declare no competing interests.

Additional information

Supplementary Information The online version contains supplementary material available at <https://doi.org/10.1038/s41598-025-91173-y>.

Correspondence and requests for materials should be addressed to M.Z. or C.L.

Reprints and permissions information is available at www.nature.com/reprints.

Publisher's note Springer Nature remains neutral with regard to jurisdictional claims in published maps and institutional affiliations.

Open Access This article is licensed under a Creative Commons Attribution-NonCommercial-NoDerivatives 4.0 International License, which permits any non-commercial use, sharing, distribution and reproduction in any medium or format, as long as you give appropriate credit to the original author(s) and the source, provide a link to the Creative Commons licence, and indicate if you modified the licensed material. You do not have permission under this licence to share adapted material derived from this article or parts of it. The images or other third party material in this article are included in the article's Creative Commons licence, unless indicated otherwise in a credit line to the material. If material is not included in the article's Creative Commons licence and your intended use is not permitted by statutory regulation or exceeds the permitted use, you will need to obtain permission directly from the copyright holder. To view a copy of this licence, visit <http://creativecommons.org/licenses/by-nc-nd/4.0/>.

© The Author(s) 2025